Tidal range structure operation assessment and optimisation

Tidal range structure operation assessment and optimisation

Athanasios Angeloudis MEng, PhD

NERC Research Fellow, Department of Earth Science and Engineering,
Imperial College London, London, UK.
a.angeloudis06@imperial.ac.uk , +44 (0) 79126 12941

Abstract

The construction and operation of tidal range structures has been in the spotlight since the UK Government-commissioned Hendry Review, published in early 2017, advised that tidal power can play a significant role in the future energy mix. These dam proposals undergo rigorous scrutiny over their feasibility and environmental implications, despite presenting opportunities to deliver sustainable large-scale electricity supplies to the national grid. Preceding efforts to harness the UK's vast untapped tidal energy resource through barrages were dismissed on the grounds of feasibility and environmental uncertainties. There is now an urgent need to develop reliable engineering tools that can be used to improve the feasibility of new designs under consideration. In this case a novel coastal ocean finite element model is coupled with tidal power plant operation algorithms. This is applied to assess the performance of tidal range structures such as the high profile infrastructure projects of the Swansea Bay and Cardiff tidal lagoons. The analysis takes into account an adaptive operation over time that aims to maximise the electricity output over variable spring-neap tidal conditions. It is demonstrated that such hydrodynamic models, when informed regarding the design of the constituent turbines and sluice gates installed, can simulate the dam's power plant operation to provide insights to the energy output and hydro-environmental impacts of such schemes.

Keywords: Tidal range energy, tidal lagoon, marine energy, resource assessment, control optimisation, gradient-based optimisation.

1. Introduction

Tidal energy is a renewable energy source that comes with complete predictability and is a result of the tide generating forces that arise from the coupled Earth-Moon system and other celestial bodies. In particular, the UK coastline offers amplifying geographical features that correspond to either strong tidal stream currents or a high tidal range. Indicatively, there is the potential to source approximately 15% and 12 % of the national electricity demand from tidal stream and range projects respectively. Given the enormous opportunity of this untapped energy resource, pilot projects for tidal stream and range based energy generation are in the advanced stages of planning and development within the UK. The first tidal stream turbines installed within a pilot array in the Pentland Firth (Martin-Short et al., 2015) off of Scotland have just started to generate power. For tidal range-based technologies, the UK Government's "Hendry review" (Hendry, 2017) published on the 10th of Feb 2017, recommended that tidal lagoons can play an important role in the UK's energy mix. This provides a roadmap towards the development of the Swansea Bay lagoon by Tidal Lagoon Power Ltd as a pathfinder project. Construction could commence in 2018, with much larger industrial projects to follow.

Assessment of tidal energy technologies and potential impacts relies on the development of numerical tools that simulate their operation over time. These can range from simplified theoretical models to more sophisticated multi-dimensional hydrodynamics packages that may require High Performance Computing to be applicable in practice (Aggidis and Feather, 2012; Wolf et al., 2009; Angeloudis et al., 2016; Neill et al., 2017; Lewis et al., 2017). In the latter case, modelling tidal range structures is particularly challenging, since hydro-environmental models need to be adapted with specialised algorithms that are tailored to the operation of the constituent hydro-turbines and sluice gates in place.

Three designs of varying scale are assessed in terms of their energy output and hydrodynamics impact. These are firstly the Swansea Bay and Cardiff tidal lagoons proposed by Tidal Lagoon Power Ltd (TLP); the two proposals are currently under consideration by the UK Government and in the advanced stages of design. The Cardiff-Weston Barrage design that was proposed by the Severn Tidal Power Group (STPG) in 1987 is also modelled as a classical example of a large scale dam project. Initially,

2-D modelling is used to simulate and understand the established tidal conditions in a computational domain that extends beyond the Bristol Channel, UK. The tidal signals predicted at sites of interest in combination with design characteristics are used to optimise the operation assuming a negligible hydrodynamic impact. In turn the outcome of the optimisation informs refined coastal models that are coupled with algorithms to simulate the performance of power plants. In this manner the energy output in time as well as the hydrodynamic impact of the schemes can be characterised.

2. Methodology

2.1. Tidal range structure case studies

The region of the Bristol Channel and the Severn Estuary in the South West of the UK is a prime location to site tidal range structures as it hosts some of the largest tidal ranges worldwide. There, a Swansea Bay Lagoon design was granted planning consent in 2015 and is suggested to have an installed capacity of 320 MW (Waters and Aggidis, 2016; Petley and Aggidis, 2016). Even though it is seen a pilot scheme, it would become the largest tidal range project to-date and will function through a two-way operation sequence with pumping intervals to both reduce power generation intermittency and benefit overall energy outputs (Yates et al., 2013). The Cardiff Lagoon is a larger scheme proposed to operate upstream the Swansea Bay Tidal Lagoon and within the Severn Estuary. A Cardiff-Weston (Severn) barrage was a detailed proposal consisting of an 8640 MW capacity, dwarfing other tidal power schemes and is treated here as an example of a large-scale scheme. The location and area covered by the tidal range structures is presented in Fig. 1.

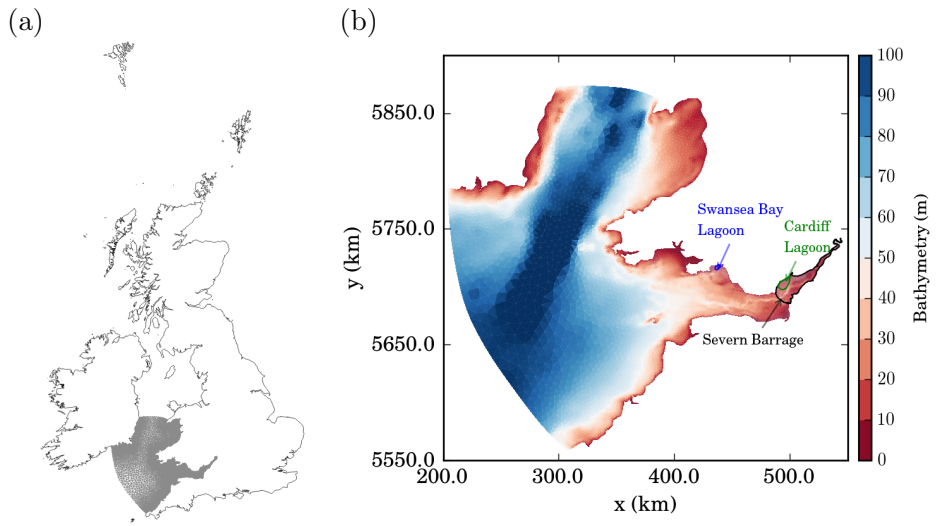

Figure 1: (a) Superimposed coastal model domain relative to the UK and (b) coastal model bathymetry interpolated from the dataset of (Edina Digimap Service, 2014) at an one arc-second resolution (≈ 30 m). Coordinates based on a UTM zone 30N projection (spatial reference EPSG:32630).

2.2. Operational modelling and optimisation

The operation of tidal range structures relies on harnessing the potential energy from water head i.e. $H = \eta_{up} - \eta_{dn}$, where η_{up}, η_{dn} are the downstream and upstream water levels relative to the structure sides. Theoretically, and assuming no losses, the potential energy available for H corresponds to:

$$E_{\max} = \frac{1}{2}\rho g A H^2 \tag{1}$$

in J where ρ is the water density (kg/m^3), g the gravitational acceleration (m/s^2) and A the impounded surface area (m^2) (Prandle, 1984). The energy that can be extracted depends on the regulation of the hydraulic structures by following a sequence of operational modes that facilitate desirable values of H for a sufficient amount of time. A generalised sequence which is adopted here is schematically illustrated in Fig. 2 with a description of the hydraulic structure parametrisations in Table 1. The P_h and Q_h hill chart values for the turbines are specific to the turbine technology and can be parametrised as per

the work of (Aggidis and Feather, 2012). Following available information on the design of the three schemes, 7.35m 20 MW, 8.9m 30 MW and 9.0 m 40 MW turbines where considered for the Swansea Bay Tidal Lagoon, the Cardiff Lagoon, and the Severn Barrage respectively. The corresponding hill charts from such specifications are provided in Fig. 3.

At this stage the dam operation can be modelled using a tidal elevation time series representing the downstream water levels (η_{dn}) (0-D modelling). This simplified modelling approach once connected with optimisation algorithms can iteratively determine the optimum scheduling parameters of Fig 2 for each tidal cycle as demonstrated in more detail in (Angeloudis et al., 2017a). The main specifications that remain constant for the three cases are summarised in Table 2 according to publicly available data, while arrays of the control values that stem from the operational optimisation are fed into the operation scheduling in the hydrodynamic modelling that is described below.

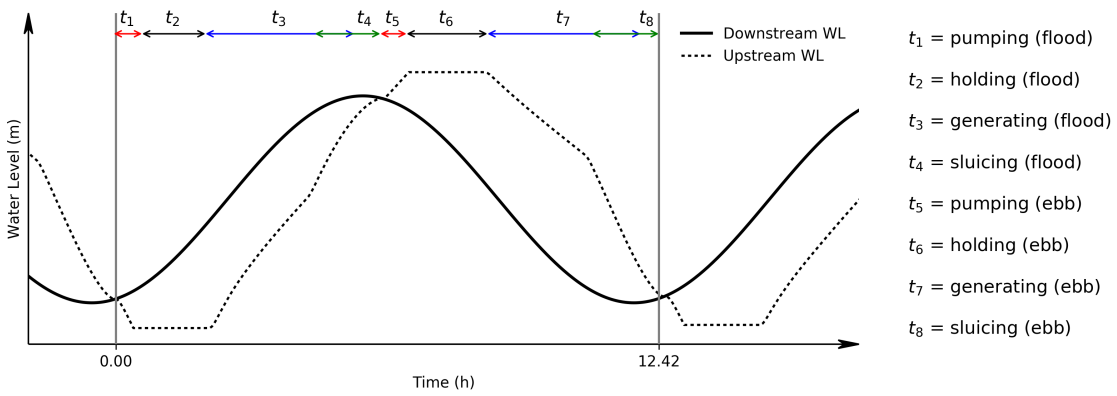

Figure 2: Generalised operation of a tidal power plant over an M_2 tidal period $\approx$ 12.42h, illustrating typical modes of operation. Red arrows represent consumption of energy, blue arrows generation periods and green the transfer of water volume from sluice gates. Adapted from (Angeloudis et al., 2017a).

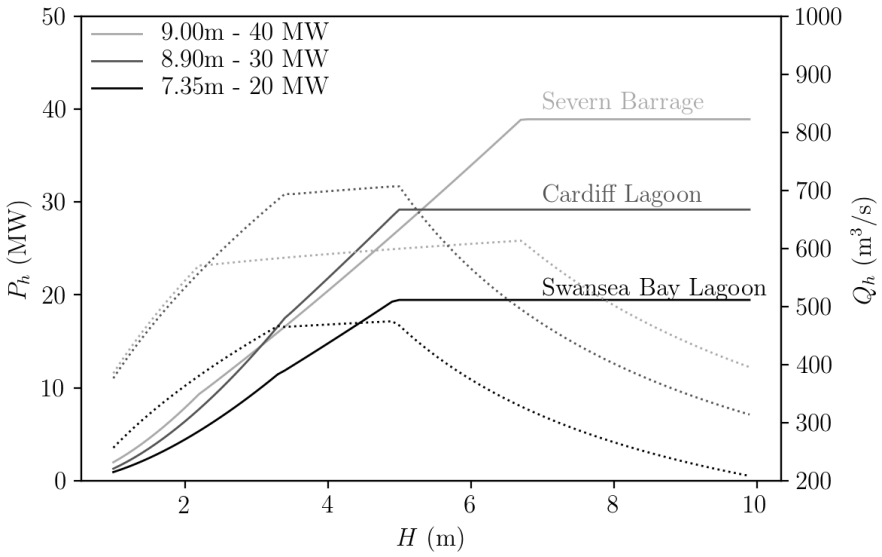

Figure 3: Hill charts parametrisations for the different turbines suggests for the three tidal range schemes. The parametrisation features a more conservative hydraulic efficiency than previously (Angeloudis and Falconer, 2017) and a sequence to calculate hill chart values can be found in (Aggidis and Feather, 2012; Angeloudis et al., 2017a).

Table 1: Control sequence and reference guide for the modes of operation m in a tidal power plant.

m	Operation Mode Description	Parametrisations
1	Pumping at flood tide (emptying)	$Q_t(m,H,t) = -r(t)\cdot \mathrm{sgn}(H)\cdot N\cdot Q_p$ $Q_s(m,H,t) = 0.0$ $P(m,H,t) = -r(t)\cdot \rho\cdot g\cdot Q_p\cdot \lvert H\rvert/\eta_p$
2	Holding at Low Water (preserving)	$Q_t(m,H,t) = 0.0$ $Q_s(m,H,t) = 0.0$ $P(m,H,t) = 0.0$
3a	Flood generation (filling)	$Q_t(m,H,t) = r(t)\cdot \mathrm{sgn}(H)\cdot N\cdot Q_h(H)$ $Q_s(m,H,t) = 0.0$ $P(m,H,t) = r(t)\cdot N\cdot P_h(H)$
3b	Flood generation with sluicing (filling)	$Q_t(m,H,t) = r(t)\cdot \mathrm{sgn}(H)\cdot N\cdot Q_h(H)$ $Q_s(m,H,t) = r(t)\cdot \mathrm{sgn}(H)\cdot C_d\cdot A_s\cdot \sqrt{2g\lvert H\rvert}$ $P(m,H,t) = r(t)\cdot N\cdot P_h(H)$
4	Sluicing (filling)	$Q_t(m,H,t) =$ $Q_s(m,H,t) = r(t)\cdot \mathrm{sgn}(H)\cdot C_d\cdot A_s\cdot \sqrt{2g\lvert H\rvert}$ $P(m,H,t) = 0.0$
5	Pumping water at ebb tide (filling)	$Q_t(m,H,t) = -r(t)\cdot \mathrm{sgn}(H)\cdot N\cdot Q_p$ $Q_s(m,H,t) = 0.0$ $P(m,H,t) = -r(t)\cdot \rho\cdot g\cdot Q_p\cdot \lvert H\rvert/\eta_p$
6	Holding at High Water (preserving)	$Q_t(m,H,t) = 0.0$ $Q_s(m,H,t) = 0.0$ $P(m,H,t) = 0.0$
7a	Ebb generating (emptying)	$Q_t(m,H,t) = r(t)\cdot \mathrm{sgn}(H)\cdot N\cdot Q_h(H)$ $Q_s(m,H,t) = 0.0$ $P(m,H,t) = r(t)\cdot N\cdot P_h(H)$
7b	Ebb generating with sluicing (emptying)	$Q_t(m,H,t) = r(t)\cdot \mathrm{sgn}(H)\cdot N\cdot Q_h(H)$ $Q_s(m,H,t) = r(t)\cdot \mathrm{sgn}(H)\cdot C_d\cdot A_s\cdot \sqrt{2g\lvert H\rvert}$ $P(m,H,t) = r(t)\cdot N\cdot P_h(H)$
8	Sluicing (emptying)	$Q_t(m,H,t) = r(t)\cdot \mathrm{sgn}(H)\cdot N\cdot C_t\cdot \sqrt{2g\lvert H\rvert}\cdot \pi D^2/4$ $Q_s(m,H,t) = r(t)\cdot \mathrm{sgn}(H)\cdot C_d\cdot A_s\cdot \sqrt{2g\lvert H\rvert}$ $P(m,H,t) = 0.0$

Q_t = cumulative turbine flowrate (m^3/s), Q_s = cumulative sluice gate flowrate (m^3/s),
P = Power consumed or generated (MW), r = ramp function at the beginning of mode,
H = head difference (m), N = turbine number, Q_p = pumping flowrate (m^3/s), η_p = pumping efficiency
P_h = power generated according to hill chart (MW), C_d = discharge coefficient, A_s = total sluice gate area (m^2)

Table 2: Tidal range structure case study specifications

Specifications	Swansea Bay Tidal Lagoon	Cardiff Tidal Lagoon	Severn Barrage
Surface area A (km^2)	11.6	64	573
Turbine number N	16	71	216
Total Capacity C (MW)	320	2130	8640
Sluice gate area A (m^2)	800	2400	35000

2.3. Hydrodynamics modelling

Regional coastal ocean models can be used to predict the flow elevations, velocities and the altered tidal constituents caused by the introduction of tidal impoundments. In this case, *Thetis* (http://thetisproject.org/), a (2-D and 3-D) flow solver for simulating coastal and estuarine flows is applied, implemented using the *Firedrake* finite element Partial Differential Equation (PDE) solver framework (Rathgeber et al., 2016). *Thetis* is configured to solve the non-conservative form of the nonlinear shallow water equations:

$$\frac{\partial \eta}{\partial t} + \nabla\cdot(H_d\mathbf{u}) = 0, \tag{2}$$

$$\frac{\partial \mathbf{u}}{\partial t} + \mathbf{u}\cdot\nabla\mathbf{u} - \nu\nabla^2\mathbf{u} + f\mathbf{u}^{\perp} + g\nabla\eta = -\frac{\tau_b}{\rho H_d}, \tag{3}$$

where η is the water elevation, H_d is the total water depth and $\mathbf{u}$ is the depth-averaged velocity vector while ν is the kinematic viscosity of the fluid. Considering the scale of the problem, one must introduce the Coriolis term $f\mathbf{u}^{\perp}$ where $\mathbf{u}^{\perp}$, the velocity vector rotated counter-clockwise over 90^o and $f = 2\Omega\sin$ with Ω the angular frequency of the Earth's rotation and ζ the latitude. Bed shear stress (τ_b) effects

are represented here through the Manning's n formulation as:

$$\frac{\tau_b}{\rho} = gn^2 \frac{||\mathbf{u}||\mathbf{u}}{H_d^{\frac{1}{3}}}. \tag{4}$$

Intertidal wetting and drying processes are represented according to the formulation of (Kärnä et al., 2011). The model is implemented using a discontinuous Galerkin finite element discretisation (DG-FEM), using the $P_{1DG} - P_{1DG}$ velocity-pressure finite element pair. A semi-implicit Crank-Nicolson timestepping approach is applied for temporal discretisation with a constant timestep of $\Delta t = 50$ s. Discretised equations are solved using a Newton nonlinear solver algorithm using the PETSc library (Balay et al., 2016). Apart from the conventionally imposed water levels at the seaward boundaries and the river discharge fluxes along the coast, the representation of the turbines and sluice gates is implemented according to a flux-based method using the principles of domain decomposition (Angeloudis et al., 2016). Associated fluxes are determined at each time step by sampling the water elevations adjacent to the turbines and sluice gates to calculate H and accordingly feed it to the parametrisations of Table 1.

Building on previous studies (Angeloudis et al., 2016; Angeloudis and Falconer, 2017; Angeloudis et al., 2017a; Falconer et al., 2009; Xia et al., 2010), the computational domain (Fig. 1b) was extended to consistently quantify the impacts of the largest of the schemes, i.e. the Severn Barrage. It should be remarked that earlier studies have extended the domain even further to the continental shelf (Zhou et al., 2014) and there are more sensitivity analyses that must be performed to find the optimum location for the seaward boundaries considering the scale of the proposed infrastructure. In this case the same extended domain was used to model the tidal range schemes in order to consistently assess the energy output and monitor changes on the tidal elevations at tide gauges within the Bristol Channel. However, the unstructured meshing capabilities also enable mesh refinement in areas of interest, i.e. close to the vicinity of turbines and sluice gates (see Fig. 4).

The simulated periods spanned two months (6/5/2003 to 6/7/2003) after being ramped up for five days to ensure independence from the model initial conditions. The models were forced at the seaward boundaries based on the constituents from the TPXO database (Egbert and Erofeeva, 2002).

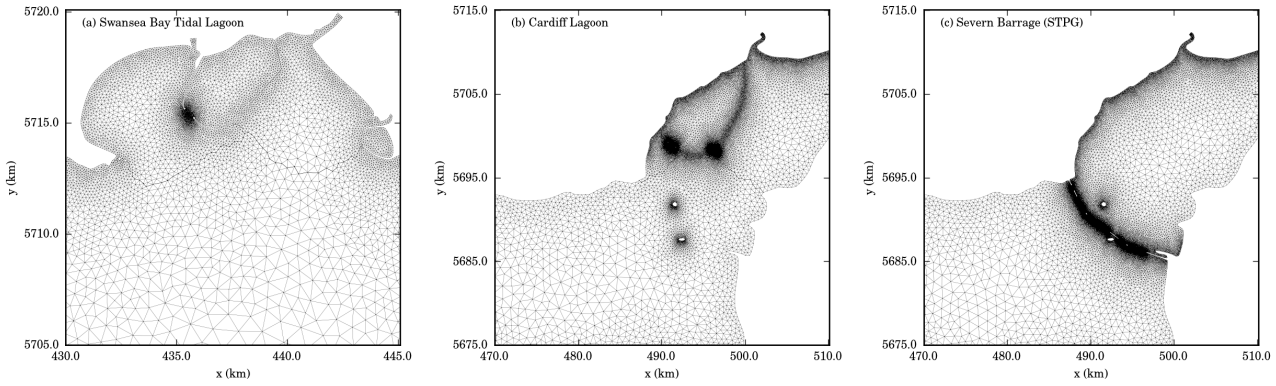

Figure 4: Mesh refinement near turbines and sluice gates for the Swansea Bay, Cardiff lagoons and the Severn Barrage STPG design.

3. Results & Discussion

3.1. Validation and hydrodynamic impact

The performance of the coastal models to simulate the tidal conditions within the Bristol Channel was benchmarked against tide gauge measurements from BODC's National Tide Gauge Network and recorded tidal constituents. A good agreement is observed for the reproduction of constituent amplitude α and phase ϕ, with the principal M_2 and S_2 components summarised in Table 3 as determined through the harmonic analysis of simulation-predicted elevation signals. Fig. 5 plots water level measurements over a spring-neap tidal cycle together with the results of a validated simulation on a smaller domain discussed in Angeloudis et al. (2017b). Even though both simulations correspond to similar agreement

regarding the tidal constituents, minor discrepancies arise in the larger model's phase during spring tides (Fig. 5). These are attributed to the way the models are calibrated as they rely on a single friction parameter that is assumed to be uniform across the domain, the Manning's n. In each case, the best agreement was delivered with n=0.023 and n=0.018 for the smaller and larger computational domains respectively. Given that the overall amplitudes and phases adequately represent the potential energy contained in the tide as in (1), the particular setup was deemed sufficient for the relative simulations that consider the three tidal range structures.

Table 3: Comparison between observed and modelled data for amplitude α (m) and phase ϕ (deg) at tide gauge stations along the Bristol Channel model

Location	M_2				S_2			
	Data		Model		Data		Model	
	α(m)	$\phi(^o)$	α(m)	$\phi(^o)$	α(m)	$\phi(^o)$	α(m)	$\phi(^o)$
Mumbles	3.116	172.5^o	3.05	155.2^o	1.106	220.3^o	1.07	202.5^o
Ilfracombe	3.043	161.9^o	2.86	152.6^o	1.112	208.7^o	1.0	199.3^o
Hinkley-Point	3.909	182.6^o	3.95	165.6^o	1.397	236.8^o	1.34	217.4^o
Newport	4.134	195.0^o	4.25	174.8^o	1.469	252.7^o	1.38	230.0^o
Avonmouth	4.262	201.6^o	4.3	182.2^o	1.497	261.6^o	1.35	239.0^o

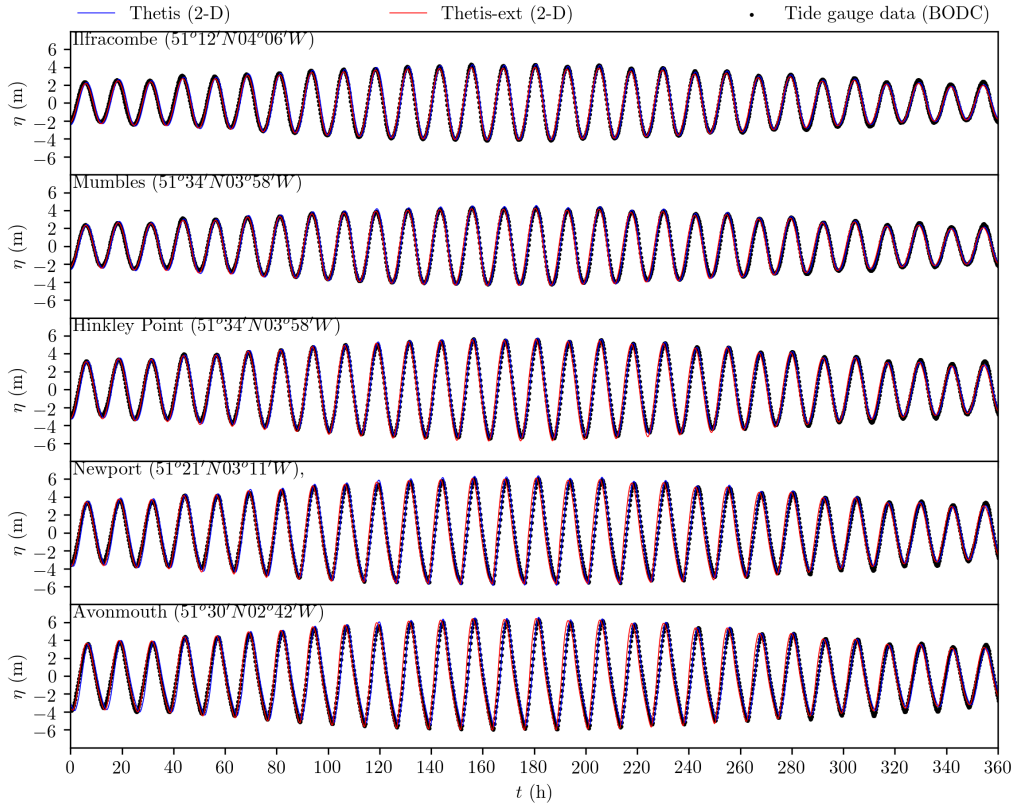

Figure 5: Validation of extended boundary simulation results (Thetis-ext) against British Oceanographic Data Centre (BODC) tide gauge data and comparison with the results of the smaller domain reported in (Angeloudis et al., 2017b).

Hydrodynamic impact was quantified by monitoring tidal constituents changes at the five tide gauges (Fig. 5) and monitor points immediately downstream of the turbine sections in relation to the established hydrodynamics simulation results, summarised in Table 3. An additional parameter to understand the cumulative impact of the schemes for the entirety of the constituents considered (9 including the shallow water constituent $M4$) is introduced. This entails the calculation of the deviation of the annual potential energy available at the sampling points (ΔE). The calculation of the quantity relies on the recursive application of Eq. 1 to the individual transitions of HW to LW over an annual period from reconstructed tidal signals of the original and altered tidal constituents. This parameter thus captures the interaction of the schemes with the hydro-environment over multiple cycles.

The introduction of the tidal structures primarily leads to both phase and amplitude differences and typically a reduction of the available potential energy of the estuary. Few exceptions appear, as the

Table 4: Change in principal constituents M_2 and S_2 by the introduction of the tidal range structures. δa represents change in amplitude in m and $\delta\phi$ phase difference in degrees. ΔE quantifies the difference in the potential energy from 8 tidal constituents and also M_4 to assess the difference in potential energy post-construction.

	Swansea Bay Lagoon				
	M_2		S_2		ΔE %
	α(m) - ($\delta\alpha$)	$\phi(^o)$ - ($\delta\phi$)	α(m) - ($\delta\alpha$)	$\phi(^o)$ - ($\delta\phi$)	
Swansea Lagoon	2.92 *(-0.10)*	158.8 *(3.04)*	1.09 *(0.04)*	206.0 *(3.85)*	-4.4
Cardiff Lagoon	4.01 *(0.00)*	171.7 *(-0.77)*	1.52 *(0.20)*	224.7 *(2.21)*	4.2
Severn Barrage	3.91 *(-0.01)*	168.6 *(-0.25)*	1.48 *(0.18)*	220.6 *(2.54)*	3.6
Mumbles	2.92 *(-0.12)*	158.3 *(3.14)*	1.06 *(-0.01)*	205.9 *(3.48)*	-6.4
Ilfracombe	2.76 *(-0.10)*	155.8 *(3.26)*	1.00 *(-0.00)*	203.0 *(3.78)*	-5.6
Hinkley-Point	3.86 *(-0.08)*	167.4 *(1.76)*	1.40 *(0.06)*	219.0 *(1.86)*	-2.5
Newport	4.18 *(-0.06)*	175.6 *(0.86)*	1.47 *(0.08)*	230.4 *(0.65)*	-1.8
Avonmouth	4.26 *(-0.03)*	182.7 *(0.50)*	1.47 *(0.11)*	239.2 *(0.56)*	0.5
	Swansea Bay & Cardiff Lagoon				
	M_2		S_2		ΔE %
	α(m) - ($\delta\alpha$)	$\phi(^o)$ - ($\delta\phi$)	α(m) - ($\delta\alpha$)	$\phi(^o)$ - ($\delta\phi$)	
Swansea Lagoon	2.79 *(-0.24)*	158.9 *(3.22)*	1.04 *(-0.01)*	204.2 *(2.04)*	-8.9
Cardiff Lagoon	3.76 *(-0.24)*	169.8 *(-2.67)*	1.40 *(0.08)*	217.0 *(-5.45)*	-13.1
Severn Barrage	3.81 *(-0.11)*	169.5 *(0.57)*	1.37 *(0.07)*	217.7 *(-0.35)*	-7.3
Mumbles	2.89 *(-0.16)*	158.0 *(2.85)*	1.04 *(-0.03)*	204.9 *(2.54)*	-9.1
Ilfracombe	2.73 *(-0.13)*	155.6 *(3.09)*	0.98 *(-0.02)*	202.2 *(3.07)*	-8.2
Hinkley-Point	3.73 *(-0.21)*	166.5 *(0.82)*	1.33 *(-0.02)*	216.2 *(-0.99)*	-9.0
Newport	4.07 *(-0.16)*	175.9 *(1.12)*	1.40 *(0.01)*	228.5 *(-1.21)*	-7.4
Avonmouth	4.16 *(-0.14)*	182.5 *(0.26)*	1.38 *(0.03)*	236.9 *(-1.76)*	-4.4
	Severn Barrage				
	M_2		S_2		ΔE %
	α(m) - ($\delta\alpha$)	$\phi(^o)$ - ($\delta\phi$)	α(m) - ($\delta\alpha$)	$\phi(^o)$ - ($\delta\phi$)	
Swansea Lagoon	2.73 *(-0.30)*	150.3 *(-5.44)*	1.27 *(0.22)*	218.4 *(16.25)*	3.3
Cardiff Lagoon	1.84 *(-2.17)*	270.1 *(97.61)*	1.24 *(-0.08)*	358.2 *(135.70)*	-57.5
Severn Barrage	3.03 *(-0.88)*	168.6 *(-0.29)*	1.49 *(0.19)*	236.4 *(18.31)*	-26.3
Mumbles	2.63 *(-0.41)*	156.2 *(0.97)*	0.94 *(-0.13)*	202.1 *(-0.26)*	-25.0
Ilfracombe	2.51 *(-0.35)*	154.3 *(1.72)*	0.90 *(-0.11)*	200.0 *(0.81)*	-22.7
Hinkley-Point	3.00 *(-0.94)*	162.0 *(-3.61)*	1.03 *(-0.32)*	209.3 *(-7.87)*	-41.4
Newport	1.85 *(-2.39)*	251.8 *(77.08)*	0.77 *(-0.62)*	321.6 *(91.82)*	-78.5
Avonmouth	1.93 *(-2.36)*	256.1 *(73.93)*	0.80 *(-0.56)*	327.4 *(88.76)*	-76.8

Swansea Bay lagoon results to a marginal increase of the tidal range at the inner Severn Estuary. The introduction of the Cardiff Lagoon compensates for these increases as it affects the tidal resonance within the estuary. Nevertheless, tidal lagoons have a drastically lesser impact than the Severn Barrage 4; this scheme would significantly alter the dynamics in the estuary (both downstream and upstream) and lead to an increase of the tidal range in the Swansea Bay area. These results are consistent with preceding assessments of the barrage (Bray et al., 2016; Angeloudis and Falconer, 2017). It should be remarked that increases in tidal range can both mean an increase for the available potential energy, but also potential implications for coastal flooding for susceptible communities.

3.2. Tidal energy output

The adaptive operation stemming from the 0-D optimisation can be appreciated in Fig. 6 where at every tidal cycle, optimised parameters are imposed to maximise energy for each cycle. An overall overview regarding how much energy can be obtained is condensed in Table 5. The adaptive operation proves beneficial for the lagoons that have a relatively contained impact on surrounding water levels. The operation leads to energy outputs in excess of 50% of the potential energy available which is superior to empirical thresholds suggested previously (e.g. 36% for a conventional two-way operation Burrows et al. (2009); Prandle (1984)). As the optimisation process does not account for the hydrodynamics changes, the sequence parameters for the barrage do not result in superior performance as the optimisation does not consider the changes predicted from the 2-D model. Ongoing research currently focuses on PDE-constrained optimisation to efficiently incorporate the hydrodynamics in the process and provide superior solution.

Overall, 54%, 52% and 16% of the respective potential energy is extracted from the Swansea Bay Lagoon, the Cardiff Lagoon and the Severn Barrage. Even though the barrage scheme performed poorly, 2-D simulations were operational and design parameters were adapted by trial and error have led to a slightly better performance in the order of 26% (Angeloudis et al., 2017a), albeit with a more ambitious hydraulic efficiency. Nonetheless, PDE-constrained optimisation approaches will be essential

for balancing the multifaceted constraints of these schemes and ensure that they meet their potential post-construction.

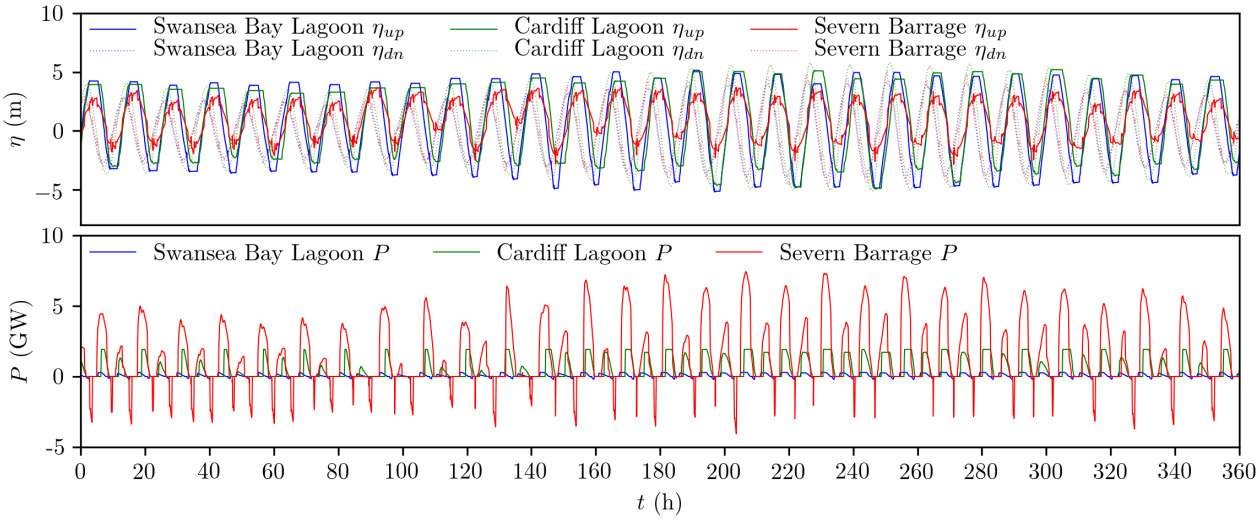

Figure 6: (a) Upstream (η_{up}) and downstream (η_{dn}) elevations predicted during the adaptive operation simulations for the three designs and (b) corresponding power outputs.

Table 5: Energy output from the three *Thetis* simulations including tidal range structures over a 2 month period. $\frac{E_{2D}-E_{0D}}{E_{0D}}$ is the deviation of 0-D and 2-D results. E_{yr} is the projected energy based on the plant performance in 2-D simulations. E_{2D}/E_{max} is the percentage of the available potential energy harnessed once acknowledging the hydrodynamics.

	E_{2D} (TWh)	$\frac{E_{2D}-E_{0D}}{E_{0D}}$ %	E_{yr} (proj.) (TWh)	$\frac{E_{2D}}{E_{max}}$ %
	Swansea Bay Lagoon			
Swansea Lagoon	0.076	-7	0.521	55
	Swansea Bay & Cardiff Lagoon			
Swansea Lagoon	0.075	-8	0.515	54
Cardiff Lagoon	0.771	-8	4.516	52
	Severn Barrage			
Severn Barrage	1.638	-52	12.06	16

4. Conclusions

A recently developed assessment and optimisation methodology has been applied to simulate the performance of a set of prospective tidal lagoons within the Bristol Channel and the Severn Estuary, in the southwest of the UK.

The computational domain of the hydrodynamic models extends beyond the Bristol Channel to the Irish Sea to minimise seaward boundary effects. Simulations span over multiple spring-neap cycles to appreciate the operation over variable tidal conditions. Results suggest that the schemes contemplated can offer considerable amounts of sustainable energy to the National Grid. However, hydrodynamic modelling indicates that large-scale deployment of tidal power plants leads to distinct changes on regional tidal dynamics.

These conditions should be appreciated through numerical models that are tailored to the study of tidal energy technologies. Therefore, research should focus on the further development of efficient optimisation tools that can adequately capture the full spectrum of the constraints and objectives of such marine infrastructure. This is imperative at this stage, as tidal energy projects promise a new dimension for the UK industry and could position it at the forefront of marine energy developments.

Notation

ΔE	Change in potential energy at a site (%)
η	Water elevation (m)
η_{up}	Lagoon/barrage upstream elevation (m)
η_{dn}	Lagoon/barrage downstream elevation (m)
η_p	Pumping efficiency
ζ	Latitude
ρ	Density (kg/m^3)
τ_b	Bed shear stress
Ω	Angular frequency of the Earth's rotation
A	Lagoon/barrage surface area (m^2)
A_s	Total sluice gate area (m^2)
C_d	Sluice gate discharge coefficient (1.0)
E_{0D}	Energy output from 0-D simulation (TWh)
E_{2D}	Energy output from 2-D simulation (TWh)
E_{max}	Potential energy (J)
E_{yr}	Projected annual energy based on simulations (TWh)
g	Gravitational acceleration ≈ 9.807 m^2/s
H	Head difference (m)
H_d	Water depth (m)
M_2	Principal lunar tidal constituent
M_4	Shallow water tidal constituent
n	Manning's number
N	Turbine number
P	Power consumed or generated (MW)
Q_h	Flowrate value from turbine hill chart (m^3/s)
Q_t	Cumulative turbine flowrate (m^3/s)
Q_s	Cumulative sluice gate flowrate (m^3/s)
Q_p	Pumping flowrate (m^3/s)
r	ramp function at the beginning of an operational mode m
S_2	Principal solar tidal constituent
P_h	Power value from turbine hill chart
$\mathbf{u}$	Depth-averaged velocity vector
$\mathbf{u}^\perp$	velocity vector rotated counter-clockwise over 90^o

Acknowledgements

I would like to thank Prof Matthew Piggott for the support and guidance over the course of this research. I am also grateful for the support of colleagues, primarily Dr Stephan Kramer and Dr Alexandros Avdis for their contributions to the open source *Thetis* and *qMesh* projects and our discussions on computational modelling. I would also like to acknowledge the financial support from two EPSRC Impact Acceleration awards made under projects EP/K503733/1 and EP/R511547/1 and the NERC grant NE/R013209/1.

References

G. Aggidis and O. Feather. Tidal range turbines and generation on the solway firth. *Ren. Energy*, 43:9 – 17, 2012. ISSN 0960-1481. doi: http://dx.doi.org/10.1016/j.renene.2011.11.045. URL http://www.sciencedirect.com/science/article/pii/S0960148111006471.

A. Angeloudis and R. A. Falconer. Sensitivity of tidal lagoon and barrage hydrodynamic impacts and energy outputs to operational characteristics. *Ren. Energy*, 114(A):337–351, 2017. ISSN 09601481. doi: 10.1016/j.renene.2016.08.033.

A. Angeloudis, R. A. Falconer, S. Bray, and R. Ahmadian. Representation and operation of tidal

energy impoundments in a coastal hydrodynamic model. *Renewable Energy*, 99:1103–1115, 2016. ISSN 18790682 09601481. doi: 10.1016/j.renene.2016.08.004.

A. Angeloudis, S. Kramer, A. Avdis, and M. Piggott. Optimising tidal range power plant operation. *Applied Energy*, (Submitted), 2017a.

A. Angeloudis, M. D. Piggott, S. C. Kramer, A. Avdis, and D. Coles. Comparison of 0-D , 1-D and 2-D model capabilities for tidal range energy resource assessments. In *EWTEC 2017*, pages 1–10, Cork, 2017b.

S. Balay, S. Abhyankar, M. F. Adams, J. Brown, P. Brune, K. Buschelman, L. Dalcin, V. Eijkhout, W. D. Gropp, D. Kaushik, M. G. Knepley, L. C. McInnes, K. Rupp, B. F. Smith, S. Zampini, H. Zhang, and H. Zhang. PETSc users manual. Technical Report ANL-95/11 - Revision 3.7, Argonne National Laboratory, 2016. URL http://www.mcs.anl.gov/petsc.

S. Bray, R. Ahmadian, and R. A. Falconer. Impact of representation of hydraulic structures in modelling a severn barrage. *Computers & Geosciences*, 89(Supplement C):96 – 106, 2016. ISSN 0098-3004. doi: https://doi.org/10.1016/j.cageo.2016.01.010. URL http://www.sciencedirect.com/science/article/pii/S0098300416300206.

R. Burrows, I. Walkington, N. Yates, T. Hedges, J. Wolf, and J. Holt. The tidal range energy potential of the West Coast of the United Kingdom. *Applied Ocean Research*, 31(4):229–238, 2009. ISSN 01411187. doi: 10.1016/j.apor.2009.10.002. URL http://linkinghub.elsevier.com/retrieve/pii/S014111870900090X.

Edina Digimap Service. Hydrospatial one, gridded bathymetry. http://digimap.edina.ac.uk/marine/, 2014. , SeaZone Solutions Ltd, Online; accessed 2017.

G. D. Egbert and S. Y. Erofeeva. Efficient inverse modeling of barotropic ocean tides. *Journal of Atmospheric and Oceanic Technology*, 19(2):183–204, 2002. doi: 10.1175/1520-0426(2002)019<0183:EIMOBO>2.0.CO;2. URL http://dx.doi.org/10.1175/1520-0426(2002)019<0183:EIMOBO>2.0.CO;2.

R. A. Falconer, J. Xia, B. Lin, and R. Ahmadian. The Severn Barrage and other tidal energy options: Hydrodynamic and power output modeling. *Science in China Series E: Technological Sciences*, 52(11):3413–3424, 2009. ISSN 1006-9321. doi: 10.1007/s11431-009-0366-z. URL http://link.springer.com/10.1007/s11431-009-0366-z.

C. Hendry. The role of tidal lagoons. Technical report, UK Government, 2017. URL https://hendryreview.com/.

T. Kärnä, B. de Brye, O. Gourgue, J. Lambrechts, R. Comblen, V. Legat, and E. Deleersnijder. A fully implicit wetting–drying method for DG-FEM shallow water models, with an application to the Scheldt Estuary. *Computer Methods in Applied Mechanics and Engineering*, 200(5):509–524, 2011. ISSN 00457825. doi: 10.1016/j.cma.2010.07.001.

M. Lewis, A. Angeloudis, P. Robins, P. Evans, and S. Neill. Influence of storm surge on tidal range energy. *Energy*, 122:25 – 36, 2017. ISSN 0360-5442. doi: http://doi.org/10.1016/j.energy.2017.01.068. URL http://www.sciencedirect.com/science/article/pii/S0360544217300683.

R. Martin-Short, J. Hill, S. Kramer, A. Avdis, P. Allison, and M. Piggott. Tidal resource extraction in the pentland firth, uk: Potential impacts on flow regime and sediment transport in the inner sound of stroma. *Renewable Energy*, 76(Supplement C):596 – 607, 2015. ISSN 0960-1481. doi: https://doi.org/10.1016/j.renene.2014.11.079. URL http://www.sciencedirect.com/science/article/pii/S0960148114008106.

S. P. Neill, P. E. Robins, A. Angeloudis, S. Ward, I. Masters, M. J. Lewis, R. A. Falconer, M. Piano, A. Avdis, G. Aggidis, P. Evans, T. A. Adcock, M. D. Piggott, A. Zidonis, and R. Ahmadian. Tidal

range energy resource and optimization - past perspectives and future challenges. *Renewable & Sustainable Energy Reviews, submitted*, 2017.

S. Petley and G. Aggidis. Swansea Bay tidal lagoon annual energy estimation. *Ocean Engineering*, 111:348–357, 2016. ISSN 00298018. doi: 10.1016/j.oceaneng.2015.11.022.

D. Prandle. Simple theory for designing tidal power schemes. *Advances in water resources*, 7(1):21–27, 1984. ISSN 03091708. doi: 10.1016/0309-1708(84)90026-5. URL http://www.sciencedirect.com/science/article/pii/0309170884900265.

F. Rathgeber, D. A. Ham, L. Mitchell, M. Lange, F. Luporini, A. T. T. Mcrae, G.-T. Bercea, G. R. Markall, and P. H. J. Kelly. Firedrake: Automating the finite element method by composing abstractions. *ACM Trans. Math. Softw.*, 43(3):24:1–24:27, Dec. 2016. ISSN 0098-3500. doi: 10.1145/2998441. URL http://doi.acm.org/10.1145/2998441.

S. Waters and G. Aggidis. Tidal range technologies and state of the art in review. *Renewable and Sustainable Energy Reviews*, 59:514–529, 2016. ISSN 13640321. doi: 10.1016/j.rser.2015.12.347.

J. Wolf, I. A. Walkington, J. Holt, and R. Burrows. Environmental impacts of tidal power schemes. *Proceedings of the ICE Maritime Engineering*, 162(4):165–177, 2009. ISSN 1741-7597. doi: 10.1680/maen.2009.162.4.165. URL http://www.icevirtuallibrary.com/content/journals.

J. Xia, R. a. Falconer, and B. Lin. Impact of different tidal renewable energy projects on the hydrodynamic processes in the Severn Estuary, UK. *Ocean Modelling*, 32(1-2):86–104, 2010. ISSN 14635003. doi: 10.1016/j.ocemod.2009.11.002. URL http://linkinghub.elsevier.com/retrieve/pii/S146350030900208X.

N. Yates, I. Walkington, R. Burrows, and J. Wolf. Appraising the extractable tidal energy resource of the UK's western coastal waters. *Phi. Trans. Royal Soc. A: Math. Phys. Eng. Sci.*, 371(1985), 2013. URL http://rsta.royalsocietypublishing.org/content/371/1985/20120181.abstract.

J. Zhou, S. Pan, and R. a. Falconer. Effects of open boundary location on the far-field hydrodynamics of a Severn Barrage. *Ocean Modelling*, 73:19–29, 2014. ISSN 14635003. doi: 10.1016/j.ocemod.2013.10.006. URL http://linkinghub.elsevier.com/retrieve/pii/S146350031300187X.